Real-time space debris monitoring with EISCAT

J. Markkanen [a], M. Lehtinen [b] and M. Landgraf [c]

[a] *EISCAT Scientific Association, Sodankylä, Finland*

[b] *Sodankylä Geophysical Observatory, Sodankylä, Finland*

[c] *ESOC, Darmstadt, Germany*

Abstract

Following a feasibility study in 2000–2001 about using EISCAT radars to detect centimetre-sized space debris in the frame of an ESA contract, we are now in the middle of a continuation study, aimed at doing the debris detection and parameter estimation in real-time. A requirement in is to "piggy-pack" space debris measurements on top of EISCAT's normal ionospheric work, without interfering with those measurements, and to be able to handle on the order of 500 hours of measurements per year. We use a special digital receiver in parallel to EISCAT's standard receiver. We sample fast enough to correctly band-pass sample the EISCAT analog frequency band. To increase detection sensitivity, we use coherent pulse-to-pulse integration. The coherent integration is build-in in our method of parameter estimation, which we call the MF-method. The method is derived via Bayesian statistical inversion, but reduces, with common assumptions about noise and priors, to minimizing the least squares norm $||z(t) - b\,\chi(R, v, a; t)||^2$, where z is the measured signal and $b\,\chi(t)$ is the model signal. Because the model signal depends linearly on the amplitude b, it is sufficient to maximize the magnitude of the inner product (cross correlation) between z and χ, the amplitude estimate is then determined by direct computation. Magnitude of the inner product, when properly normalized, is the MF. To construct an appropriate set of model signals, we sample the EISCAT transmission, in the same way as we sample the received signal, and apply linearly changing Doppler-shifts (chirps) on it. Our original implementation of the MF-method was about four orders of magnitude too slow, but we have now gained the required speed factors. A factor of ten comes from using faster computers, another factor of ten comes from coding our key algorithms in plain c instead of Matlab. The largest factor, typically 100–300, comes from using a special, approximative, but in practice quite sufficient, method of finding the MF maximum. Test measurements show that we get real-time speed already when using a single PPC Dual Processor 2GHz G5 Macintosh to do the detection computations.

Key words: coherent integration, space debris, statistical inversion

1 Introduction

It is estimated that there are approximately 200 000 objects larger than 1 cm currently orbiting the Earth, as an enduring heritage of four decades of space activity. This includes the functioning satellites, but by far most of the objects are what is called space debris (SD), man-made orbital objects which no longer serve any useful purpose. Many of the small-sized (less than 10 cm) particles are due to explosions of spacecraft and rocket upper stages, but there are also exhaust particles from solid rocket motors, leaked cooling agents, and particles put into space intentionally for research purposes. The large (> 10 cm) objects have known orbits and are routinely monitored by the U.S. Space Surveillance Network, but information of the smaller particles is fragmentary and mainly statistical. Especially, in Europe there is no radar that is routinely used for monitoring small-size SD.

From 2000, we have been involved in two studies, contracted by ESA (ESOC, 1999, 2003), to start utilizing the EISCAT ionospheric research radars also for space debris measurements. Since the early 1980's, the EISCAT mainland radars have been performing ionospheric measurements at least 2000 hours per year; and since late 1990's, after the EISCAT Svalbard radar became operational, EISCAT has measured more than 3000 hours per year. The aim is to be able to use a substantial amount of these operating hours for simultaneous space debris measurement. In our initial study (Markkanen et al., 2002), we showed that it is feasibility, and indeed technically straightforward, to run SD measurement in parallel with normal EISCAT ionospheric measurements, without interfering with those measurements.

Our approach is to operate a separate digital receiver back-end, which we call the SD receiver, in parallel with EISCAT standard digital receiver. This allowes us to implement our own, amplitude domain data processing, the match function or matched-filtering (MF) method. The MF-method seeks to increase detection sensitivity by implementing pulse-to-pulse coherent integration. To make the hardware as simple and cheap as possible, the custom-made part of the SD receiver is basically just a fast sampler and digital demodulator; the interesting processing is done in fast but still cheap general purpose workstations. The SD receiver samples the analog IF2 band fast enough to capture all the relevant EISCAT frequency channels into a single digital stream, without doing channel separation. Typically during a measurement, we sample with the rate of about a million complex samples per second continuously, producing more than 10 Gbytes of data per hour. Early on, ESA suggested that we should strive to do data analysis in real time so that the raw data could be quickly disregarded. We describe the basics of the SD receiver in section 3.

A straightforward implementation of the MF-method implies long data vec-

tors, with lengths of hundreds of thousands complex points, to be Fourier-transformed a few thousand times, per every second of raw data. At the Space Debris III conference in 2001, we had to concede that with the processing speed that we had achieved at the time, it would take several centuries of CPU time to analyze just one year's quota of EISCAT space debris measurements. However, soon afterwards, one of us (Lehtinen), realized that by accepting some loss of detection sensitivity and a changing bias in the velocity estimate, it would be possible to speed up MF computation drastially, typically by more than two orders of magnitude. We use the term fast match function algorithm (FMF) for the resulting computation scheme. We outline the algorithm in section 8 of this paper.

The results of the initial study were encouraging. The achieved detection sensitivity was equivalent to being able to observe spherical targets with diameters of about 2 cm from 1000 km range. With the advent of the FMF algorithm, the processing speed, though still sluggish, was starting to become useful. In 2003, ESA commenced a new study with us to bring the analysis of large amounts of EISCAT SD data up to real-time speed. The study has achieved the required processing speed. In addition to the factor of 100 delivered by the FMF algorithm, we now use computers that are about ten times faster than what we had available in 2001. A final required factor of ten to the speed was obtained by coding the MF- and FMF-algorithms in c, instead of using Matlab as was done in the initial study.

The EISCAT system (Byron, 1984, 1986; Wannberg et al., 1997) consists of three separate radars: monostatic VHF radar, located near Tromsø, Norway, and operating at 224 MHz; monostatic but two-antenna EISCAT Svalbard Radar in Longyerbyen, Svalbard, operating at 500 MHz; and tristatic EISCAT UHF radar at 930 MHz, with transmitter in Tromsø and receivers in Tromsø and in Kiruna, Sweden, and Sodankylä, Finland. All the transmitters operate in the megawatt peak power range and routinely utilize high (10–20%) duty cycles.

Even though routinely picking-up hard target echoes [1] , standard EISCAT data processing is not optimized for hard targets. The characteristic feature expected from small hard targets is long signal coherence time, several hundred milliseconds. By a signal's (phase-) coherence we mean that the signal phase $\phi_0(t)$ obeys a deterministic functional form for some duration of time, called the coherence time.

EISCAT$'s$ normal ionospheric signal has coherence time less than a millisecond in most parts of the ionosphere. This time is much shorter than the interval between transmitted pulses, which in EISCAT typically is 3–10 ms. Therefore,

[1] Always termed, confusingly, "satellites" in the EISCAT parlance.

echoes from individual pulses are uncorrelated, and can only be added up in the power domain. This is done by computing, for each of the received pulses separately, signal autocorrelation functions, or, equivalently, power spectra, for a set of range gates, and then adding these power-domain quantities. This is called non-coherent pulse-to-pulse integration. Even though it is not perhaps always appreciated, we want to emphasize that within a *single* transmission/reception (T/R) cycle, computing range-gated power-spectra achieves coherent integration. In fact, for a single uncoded pulse, our MF-method, too, in effect just computes range-gated power spectra.

To achieve coherent integration from pulse to pulse, the MF-method adds the echos from different T/R cycles in amplitude domain, taking care that the pulses are added with equal phase. The method, in essence, removes *all* phase variation from the signal before adding the samples. This is achieved by guessing the phase factor $e^{i\phi_0(t)}$ of the signal, and canceling it by multiplying the signal by the complex conjugate of the guess, $e^{-i\phi_0(t)}$. The guesses in our implementation are generated by brute force. We search through a large set of parametrized model functions, and use the one which achieves best cancellation of the phase, that is, which results in largest integrated amplitude. After the phase variation has successfully been removed, the remaining part of the signal can be safely integrated, both within a single pulse, as well as from pulse to pulse. Incidentally, dividing the radar data into T/R cycles is artificial from the MF-method point of view. It is more natural to consider the totality of transmission during an integration period as just a waveform pattern, to be matched against the totality of reception, irrespective of how the patterns are chopped to T/R cycles. In particular, there is no need for the T/R cycles to be identical, neither in terms of length nor transmission content.

As long as the signal stays coherent (obeys the assumed model), coherent integration suppresses the non-coherent background noise, so that the effective signal-power to noise-power ratio increases directly proportionally to the number of pulses integrated. This increases detection sensitivity. Non-coherent integration, instead, does not increase signal-to-noise ratio. The drawback in coherent integration, in addition of it being computationally more demanding due to the long data vectors, is that if the signal model is not accurate, the ensuing phase error will quickly eat into the integrated signal amplitude, and can actually start to reduce the amplitude. [2] In our case, coherent integration beyond about 300 ms does not seem to improve detection sensitivity.

[2] And long enough integration will kill the amplitude altogether, by the Riemann-Lebesgue lemma. We admit that there is a grain of truth in the statement claiming that "most radars utilize non-coherent integration", because "maintaining coherency [...] is very costly and challenging to achieve." (Mahafza, 2000)

Part of the reason for the unexpectedly short apparent coherence time is that, although we in (see section 6) will derive a model signal that we believe should be quite accurate for small (structureless) targets, for performance reasons we cannot actually use the ideal model. The approximative model that we do use, both in the MF and FMF algorithms, is suitable for single-frequency-channel transmissions. The different frequency channels in our multi-frequency signal will have slightly different Doppler-shifts because the Doppler-shift depends on transmission frequency. It is impossible to cancel the Doppler phase factors simultaneously using only the single model phase factor which is available in the approximative model.

We derive, in section 4, the MF-method via Bayesian statistical inversion (Lehtinen, 1986). Within the Bayesian approach, the estimates for the basic parameters range, radial velocity, radical acceleration and signal amplitude (or signal total energy), are be found as the most probable values, given the measured noisy signal. With our assumptions, this solution is also the the one that minimizes the least squares norm between the measured signal and the set of model functions.

We have, during several test campaigns over four years, collected and analysed about 50 hours of data at the EISCAT UHF radar in Tromsø. This data has been taken mostly for method development and verification purposes. We will not attempt to describe the data in this paper, but only mention here that the mean event rate slightly has been slightly more than 20 events per hours. Our observed height distribution seems to reproduce the well-known main features of SD distribution in low Earth orbit region. Our measurements cover altitude up to about 4000 km, with some gaps that depend on the EISCAT experiment we have been hooked to. The data has also shown that the EISCAT UHF radar can observe targets with effective diameters (diameter of a hypothetical spherical target that would be on the antenna optical axis and would give the observed signal strength at the observed range) about 2–2.5 cm at 1000 km range.

However, we cannot say anything much about the actual target cross sections, let alone target physical diameters. The single major deficiency in EISCAT, in comparison with other radars used for space debris observations, is that EISCAT antennas do not have monopulse feed. At the moment at least, there is no way available that would allow pinpointing the actual direction of a target within the radar beam, and so the target's radar cross section cannot be deduced from the signal strength. We hope that in future we can partly alleviate this problem by collecting fairly large amounts of data—perhaps about 500 hours per year—so that the antenna beam pattern can be taken into account statistically, and meaningful comparisons to space debris models made.

2 EISCAT UHF Radar

So far in our measurements, we have been using mainly the EISCAT UHF radar. Block diagram of the UHF-radar's Tromsø site is shown in Fig. 1. The EISCAT receivers at all three UHF sites, Tromsø, Kiruna, and Sodankylä, are almost identical, the main difference being that at the receiving-only sites Kiruna and Sodankylä there is no need for the duplexer and the receiver protector. Also the polarizer arrangements are somewhat different. The Tromsø UHF receiver has a cooled preamplifier, giving system temperature $T_{\mathrm{sys}} \approx 110$ K. Kiruna and Sodankylä have recently moved over to HEMP-based, uncooled preamplifiers, with system temperatures around 50 K. The radar's RF band is centered at 929 MHz, and there are 14 transmission frequencies available, 300 kHz apart. In the most common EISCAT experiment modes, two frequency channels are used. Recently those have been centered at 929.9 MHz (EISCAT frequency F13) and 930.2 MHz (F14). The RF signal is mixed in two stages to the second intermediate frequency (IF2) band, using local oscillators at 812.0 MHz and 128 MHz, so that F13 maps to 10.1 MHz and F14 to 9.8 MHz. The band is formed by the radar's antialiasing filter, which is 6.8 MHz wide and centered at 11.25 MHz.

In the standard EISCAT data processing, the second IF is digitized by a 14-bit A/D converter, which produces a continuous sample stream at the rate of 15 Msamples/s. The stream of IF2 samples is distributed to the multi-channel, VME-based, EISCAT digital receiver, each channel taking one slot in a VME crate. Custom hardware on each digital channels performs quadrature detection, followed by sampling rate reduction appropriate to the typical 10–50 kHz final channel bandwidth. The baseband sample stream is buffered, and further processing to averaged sample correlation products is done on UNIX-based computers (EISCAT uses computers based on SPARC-processors, and the Solaris flavours of UNIX).

The EISCAT UHF transmitter consists of a programmable radar controller that generates the pulse patterns at DC level, either uncoded on/off pulses or various classes of binary phase codes; an exciter system that converts the radar controller output to RF around 928 MHz; and a klystron power amplifier that consists of two klystron tubes, in principle able to deliver combined peak power of about 2.5 MW. The power during all our space debris measurement has been considerably lower, at about 1.5 MW. The maximum transmitter duty cycle is 12.5%, and duty cycles near this value are also used in most experiments in practice.

The 32 m UHF antenna has a fully steerable parabolic dish, has Cassegrain optics, and has rotation rate of about 80°/min both in azimuth and elevation. The antenna pointing direction is calibrated using celestial radio sources, and

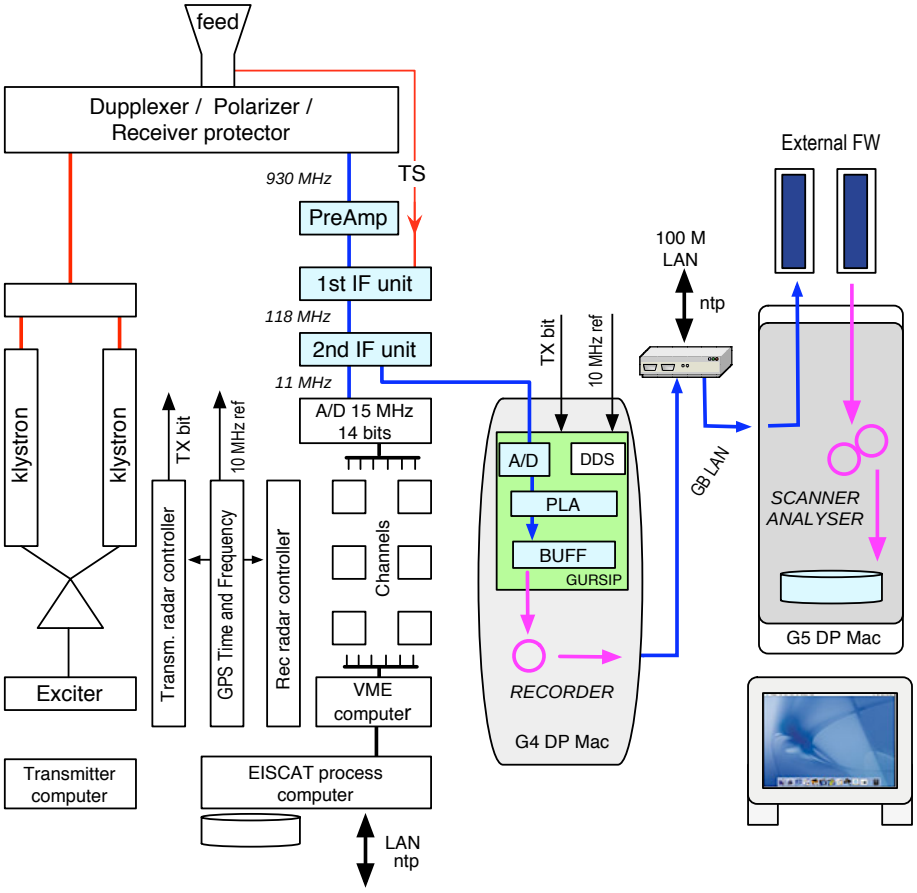

Fig. 1. The space debris receiver connected to EISCAT UHF radar.

is believed to be accurate slightly better than 0.1° in most directions. The time and frequency base at all EISCAT sites is from the GPS system.

3 Space debris receiver

To be able to use our own data processing, optimized for hard targets, we use a special digital receiver back-end, the space debris receiver. Signal to the space debris receiver is branched off from the EISCAT analog signal path at the second IF (IF2) level. Figure 1 shows the main blocks of the SD receiver, connected to the EISCAT UHF system at the Tromsø site.

EISCAT standard measurement modes normally have more than one frequency channel. EISCAT standard data processing handles this situation in the traditional way, by feeding the IF2 data to multiple hardware channels, each tuned to a particular center frequency. The end result is several sample streams, one for each channel. Our approach in the SD receiver is different.

We sample fast enough to capture the relevant part of the analog IF2 band into a single digital stream. According to the (bandbass-) sampling theorem, if the spread of frequencies is B MHz, we need to take B million complex samples per second, in the minimum. For our most often used measuring mode, where there are two frequency channels 300 kHz apart, we have normally used 500 kHz sampling rate. But we have also verified that the SD receiver can handle sampling speeds up to 2.5 Msamples/sec. We call this type of data multichannel complex data (Lehtinen, 2002).

In addition to the standard reception, our data processing requires that the transmission waveform is measured. As indicated in Fig. 1, EISCAT provides the transmission sample signal (TS) time-multiplexed into the same data path as the reception. The multiplexer switch is controlled by the receiver protector bit ("Txbit" in the figure), generated by the EISCAT radar controller microprocessor. We routinely record the receiver protector bit into our data stream to mark out the transmission blocks. The bit is stored into the least significant bit of the imaginary part of the $16 + 16$-bit complex integer data words. With this arrangement, the transmission sample signal gets automatically sampled with the same sampling rate as the actual reception (though we would actually like to sample it with a higher rate).

The core of the data acquisition system is a custom PCI-board which performs signal sampling, quadrature detection and sampling rate reduction. The board was developed originally for ionospheric tomography by the now defunct Finnish company, Invers Ltd.

The A/D converter on the PCI board samples at 40 MHz. The resulting real-valued sample stream is processed by programmable logic chip, from the Xilinks SpartanXL family, to perform quadrature detection, essentially by doing Hilbert transform. The result of the transform is a complex-valued 10 MHz sample stream, which represent the negative frequency part of the spectral contents of the analog input. The chip then decimates the 10 MHz stream to the final sampling rate. Typical decimation factor M is 20, which yields 500 kHz final sampling rate. The decimation is done by adding samples in blocks of M; this ensures proper filtering.

It may be noted that there is no separate multiplication to baseband in this scheme. Instead, the customary frequency component at baseband is created by the undersampling. With 40 MHz raw sampling, the arrangement requires that the band-limited analog input is centered at 10 MHz. Although it is possible to run the A/D converter on the board at other sampling rates, the 40 MHz is a most convenient choise. That the two frequencies EISCAT nowadays most often use in the standard measurements, are 10.1 MHz and 9.8 MHz, is a very happy coincidence indeed. Next version of the SD receiver will have a complex mixer build-in.

The PCI board is mounted on a Power Macintosh G4 workstations, running under the Mac OS X version of UNIX. The Mac G4 we call the measurement computer. In addition, there is a dual CPU Macintosh G5 computer for data analysis, and a second G5 analysis computer is forthcoming. The Mac workstations are connected to each other via a gigabit Ethernet link, and are also connected to the site LAN. The measurement computer runs software from Invers Ltd to read the sample data from an onboard buffer and write them to hard disk, either local disk, or (normally) a disk mounted over the gigabit link from the analysis computer. Data accumulation rate to hard disk is between 7 and 30 Gbytes per hour, depending on the sampling rate. The LAN connection is used to access the EISCAT process computer, to update the time base on the G4 and G5 once every 5 minutes, using the ntp protocol. This ensures that the time base in the Mac's stays within 20 ms from the time kept in the EISCAT system. This is more than adequate for time-stamping the space debris events.

Data analysis is done by c- and Matlab-programs running on the analysis computer. First, a *scanner* reads a segment (typically 300 ms) of raw data from disk, and searches though the segment for hard targets, using threshold detection within the framework of the match function method. When the threshold is exceeded, we call this a *hit*. The scanner saves the hit's description to a file, and proceeds for next data segment. A second program, the *event archiver*, inspect the list of hits trying to combine to an *event* the hits that correspond to a single target passing though the radar beam. Having determined the time boundaries of the event, the archiver copies raw data belonging to the event to a separate event directory, and goes looking for more events. Finally, the *analyser* picks events from the event directories, and deduces and saves the event parameters.

By far the most time-consuming step in the dada analysis is the scanning. Scanning is done by a c-program that makes use of the AltiVec vector processor onboard the G5, by calling routines in Apple's DSP library (vdsp), most especially the FFT routine.

The event-archiver is also a c-program, but is not performance critical. Most of its time goes to data copying, so the speed is mainly limited by disk speed. We have saved all raw data from all our test measurements so far—somewhat less than a terabyte—but in routine measurements, at most the raw data of events will be saved. With the event rates observed in test measurements, saving all events from all the $\approx$ 400 hours of space debris measurements that we anticipate to be able to do annually, would require (only) in the order of a terabyte of storage per year.

The way to compute the final target parameters is still under development. What the analyser now does, is basically to call the scanner to rescan the data,

with maximal time and range resolution but over a narrow range interval, and then make linear or quadratic fits to the range and Doppler-velocity time series. The range and velocity parameters that we normally quote are then taken from these fits, for the time instant of maximum signal strength. The analyser is a Matlab program.

The overall processing speed is such that for data taken with 2 MHz sampling rate, it takes 40–45 minutes to scan, archive and analyse one hour of raw data, while keeping the raw data access running at the same time.

4 The match function method

We want to estimate the parameters of a hard target echo signal $s(t)$ in the presence of gaussian noise $\gamma(t)$, in an optimal way. We denote by $z(t)$ the received signal,

$$z(t) = s(t) + \gamma(t)\,. \tag{1}$$

We denote by $x(t)$ the transmission sample signal. We ignore the frequency translations done in the actual space debris receiver, and treat all these quantities as complex-valued (detected) waveforms. The frequency translations affect both the signal s(t) and the transmission signal x(t) by a factor of form $\exp(i\omega_{LO}t)$, where ω_{LO} is some local ocillator frequency, and hence cancel out of the products $s(t)\overline{x(t)}$.

To find an optimal estimate (or at least a well-defined estimate), we will use the approach of Bayesian statistical inversion. The basic idea is to use a parametrized model for the signal $s(t)$ and find the most probable signal among the model signals, given the measured signal.

We specify our set of model signals explicitly in section 6. Here we will make use only of the property that the model depend linearly on one parameter, the complex amplitude b, and non-linearly on a set of the other parameters (R, v and a in our case), which we collectively denote by θ, so that

$$s(t) = b \cdot \chi(\theta; t). \tag{2}$$

We sample the signal $z(t)$, using sampling interval τ, and get N_{c} samples during a time interval T_c, which we call the integration time. Each of N_{c} the samples is a "measurement".

It makes sense that after a specific measurement z, some parameter (b, θ) values should be considered more likely than others, in a way that depends

on z. That is, the probability of the various imaginable values should be describable by some conditional probability density, with z in the condition. In the Bayesian worldview, that density is termed the *posteriori density*, and is denoted here by $D_{\mathrm{p}}(b, \theta|z)$. The *inversion problem* is to utilize the measurements to find the posteriori density. The posteriori density is the most complete inference that can be made about the parameter values, based on the measurements. Normally one wants to condense the inference to single numbers, the parameter estimates. There is no unique way to select "best" estimates, but the standard Bayesian criterion is to use the most probable values, and that is what we will use. In our case, the estimates $\widehat{b}$ and $\widehat{\theta}$ therefore are

$$(\widehat{b}, \widehat{\theta}) = \arg\max_{b,\theta} D_{\mathrm{p}}(b, \theta|z). \tag{3}$$

We now derive the posteriory density. We denote by $D(z_n|s_n)$ the conditional probability density function (PDF) of z_n, given s_n. This is just the PDF of the noise,

$$(z_n|s_n) = \frac{1}{\pi\sigma^2} \mathrm{e}^{-\frac{1}{\sigma^2}|z_n - s_n|^2}. \tag{4}$$

We assume that the noise is white, so that the noise samples are uncorrelated. Then the conditional joint PDF to produce a particular measured vector z, if the actual signal vector is s, is

$$D(z|s) = \prod_{k=0}^{N-1} D(z_k|s_k) = \frac{1}{(\pi\sigma^2)^N} \cdot \mathrm{e}^{-\frac{1}{\sigma^2}\|z-s\|^2}. \tag{5}$$

The density $D(z|s)$ is called the direct theory. Given the direct theory, the Baysian solution to our inversion problem is

$$D_{\mathrm{p}}(b, \theta|z) = C'(z) \cdot D_{\mathrm{pr}}(b, \theta) \cdot D(z|s). \tag{6}$$

Here $C'(z)$ is normalization factor. The new factor, $D_{\mathrm{pr}}(b, \theta)$, is called the prior density or a priori density. The prior density is a weight that can be used if it is known a priori— before making the measurement—that some particular signals $s(b, \theta)$ tend to occur more frequently than some others. Using D_{pr} might actually make sense when measuring space debris, to throw out detections with highly unlikely parameters. But so far we have used constant priors. For constant prior, it follows from Eq. (6) and Eq. (5) that the sought-for posteriori density is

$$D_{\mathrm{p}}(b, \theta|z) = C(z) \cdot \mathrm{e}^{-\frac{1}{\sigma^2}\|z - b\cdot\chi(\theta)\|^2}. \tag{7}$$

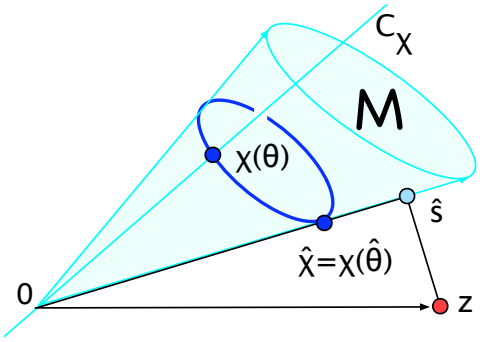

Fig. 2. Geometric interpretation of the MF-method.

It follows that finding the most probable parameters amounts to minimizing the least-squares norm,

$$(\widehat{b}, \widehat{\theta}) = \arg\min_{b,\theta} \|z - b \cdot \chi(\theta)\|^2 \,. \tag{8}$$

That we should arrive at this most basic technic of parameter estimation, least-squares fitting, is perhaps not surprising. But what we have gained by walking though the Bayesian route, is that not only do we have a method for acquiring the parameter estimates, but we have an explicit expression for the posteriori density. In the future, we intend to make use of the posteriori density in error analysis. Due to highly non-linear dependence of the model functions $\chi(\theta; t)$ on the parameters-to-be-fitted, θ, error estimation is not trivial.

A straightforward approach to the minimization problem expressed in Eq. (8) is to discretize the parameter space and perform an exhaustive search. We now show that the search space dimension can be reduced by one by making use of the property that the amplitude b enters the problem linearly. The result can be confirmed analytically, but will be here reasoned from basic vector geometry. Referring to Fig. 2, the set $\mathcal{M}$ of model vectors $\{b\,\chi(\theta)\}$ consists of 1-dimensional rays C_χ though the origin of N-dimensional complex vector space C^N. The rays are generated by the set of vectors $\chi(\theta)$. We want to find the shortest distance between the measurered point z and $\mathcal{M}$. (Due to noise, in most cases, z is outside $\mathcal{M}$ as depicted. It can also by accident be in $\mathcal{M}$, but that does not change the argument.) We need first to find the ray, $\mathrm{C}_{\widehat{\chi}}$, that is as parallel as possible with the vector z. Then the point in $\mathcal{M}$ that is nearest to z is the orthogonal projection $\widehat{s}$ of z onto $\mathrm{C}_{\widehat{\chi}}$ (a theorem in linear algebra says that the orthogonal projection gives the shortest distance of a point from a linear subspace; and the rays are linear subspaces), and is computed in the standard way as

$$\widehat{s} = \frac{\langle z, \widehat{\chi} \rangle}{\|\widehat{\chi}\|^2} \widehat{\chi} \,. \tag{9}$$

So the real problem is to find $\widehat{\chi}$. With z fixed, a sufficient measure of parallelism of a ray $C_{\chi(\theta)}$ and the vector z is the length of orthogonal projection of z onto χ; the ray is the more parallel or antiparallel, the longer the projection. We call this measure of parallelism the *match function* [3], MF. We have

$$\mathrm{MF}(\theta) = \frac{|\langle z, \chi(\theta)\rangle|}{\|\chi(\theta)\|}\,. \tag{10}$$

The notation indicates that the MF is a function of the parameter θ that determines the vector χ. Note that the MF does not depend on the scale of χ (χ and $a\,\chi$ give the same value of MF). We need to maximize the MF to get the maximally parallel model vector $\widehat{\chi} = \chi(\widehat{\theta})$:

$$\widehat{\theta} = \arg\max_{\theta} \mathrm{MF}(\theta)\,. \tag{11}$$

How the maximum is computed in practice will be discussed later in detail; basically, we performing an exhaustive search over a grid of values of θ.

The energy [4] of any correctly sampled complex-valued signal $x(t)$ is

$$W_x = \int |x(t)|^2 dt = \tau \sum |x_n|^2 = \tau \|x\|^2\,. \tag{12}$$

From Eq. (9)–(11), the energy $W_{\widehat{s}}$ of the estimated signal $\widehat{s}$ is

$$\frac{W_{\widehat{s}}}{\tau} = \|\widehat{s}\|^2 = \frac{|\langle z, \widehat{\chi}\rangle|^2}{\|\widehat{\chi}\|^2} = [\mathrm{MF}(\widehat{\theta})]^2 = \max \mathrm{MF}^2. \tag{13}$$

We normally use $W_{\widehat{s}}$ as our estimator of the signal energy. However, as will be discussed shortly, the estimator contains traces of the noise background, and is a biased estimator.

We summarize the match function method of parameter estimation

[3] Intuitively, the more parallel two signal vectors (functions) are, the more they look alike, which is one reason for our nomenclature. A more serious reason is that "MF" also stands for Match Filter. With velocity and acceleration fixed, so that MF is function of the range variable only, $R \to \langle z, \chi(R)\rangle$ amounts to ordinary filtering of z by the filter $h(t) = \chi(0)(t)$ which is matched to the transmitted signal. The MF is a generalization of this concept to more general kind of pattern matching.

[4] We consider the signals $x(t)$ to have the dimension of voltage, and assume unit impedance, so that $|x|^2$ is the signal power. The impedance does not matter, for only signal ratios, like $|s|^2/|\gamma|^2$, are used when comparing to the physical world. We could also do without explicitly tracking the sampling interval, except that we do not want to change the dimension of energy in the *middle* of a chain of equations.

(1) Get the parameter(s) θ by locating the *position* of MF maximum, Eq. (11).
(2) Get the signal energy as the square of the *value* of the MF maximum, Eq. (13).

According to Eq. (9), the complex amplitude b is be estimated as

$$\widehat{b} = \frac{\langle z, \widehat{\chi} \rangle}{\|\widehat{\chi}\|^2}, \tag{14}$$

but because the scale of the $\widehat{\chi}$ is arbitrary, so is the scale of $\widehat{b}$. Only the product $\widehat{s} = \widehat{b}\widehat{\chi}$ is well-defined.

A noise-free MF is useful for theoretical considerations. Without noise, both factors in the inner product in Eq. (10) are model functions. We will reserve a separate notation, AF, and use the standard name, *ambiguity function* (Skolnik, 1981), for our noise-free match function,

$$\mathrm{AF}(b_0, \theta_0; \theta) = \frac{|\langle b_0\, \chi(\theta_0), \chi(\theta) \rangle|}{\|\chi(\theta)\|}\,. \tag{15}$$

In the MF-method, target detection is based on the estimated signal energy $W_{\widehat{s}}$ exceeding a threshold. Setting the threshold has so far been done by visual inspection of the data, to be so high that there are only very few false alarms. In fact, we need to use a range-dependent threshold, because the lower altitudes, typically up to about 500 km, are often "contaminated" by strong clutter from ionosphere, and need a higher threshold.

The threshold is set in terms of the ratio of signal energy to the noise power spectral density (PSD) G_γ. We call this ratio the *energy-to-noise ratio*, and denote it by $\mathrm{SNR_N}$,

$$\mathrm{SNR_N} = \frac{W_s}{G_\gamma}\,. \tag{16}$$

We assume that the system noise temperature T_{sys} is defined in such a way that the noise PSD density of complex-valued wide-band noise can be written as

$$G_\gamma = kT_{\mathrm{sys}}\,, \tag{17}$$

where k is the Boltzman constant. The power of such a noise after being filtered with a boxcar-shaped low-pass filter that extends from frequency $-B/2$ to $B/2$ is

$$P_\gamma = kT_{\mathrm{sys}}B. \tag{18}$$

We call B (rather than $B/2$, as is often done in the literature) the filter bandwidth, and the noise bandwidth. We assume that the sampling interval τ and noise bandwidth are related by

$$B \cdot \tau \approx 1. \tag{19}$$

In the MF-method, we get an estimate of the energy-to-noise ratio from the MF maximum value and from separately estimated noise power:

$$\frac{W_{\widehat{s}}}{kT_{\mathrm{sys}}} = \frac{W_{\widehat{s}} \cdot B}{kT_{\mathrm{sys}} \cdot B} = \frac{(\max \mathrm{MF}^2 \cdot \tau) \cdot (1/\tau)}{P_\gamma} = \frac{\max \mathrm{MF}^2}{P_\gamma}. \tag{20}$$

We treat the system temperature as a known, fixed radar parameter, and use Eq. (20) to find the signal energy in physical units. We use that estimate to find a lower limit, $\mathrm{RCS}_{\mathrm{min}}$, for the target's radar cross section (RCS). From the standard radar equation it follows

$$\mathrm{RCS} = \frac{(4\pi)^3\, kT_{\mathrm{sys}} \cdot R^4 \cdot \mathrm{W_s}}{G(\phi)^2 \cdot \lambda^2 \cdot P_x \cdot \mathcal{D}T_c}\,. \tag{21}$$

Here R is target range, λ is radar wavelength, P_x transmission power, $\mathcal{D}$ transmission duty cycle so that $\mathcal{D}T_c$ is the actual length of transmission during the integration T_c. The factor $G(\phi)$ is the antenna power gain in the direction of the target within the radar beam, an angle ϕ offset from the known direction of the antenna optical axes. (The direction of the optical axis is known to an accuracy of about 0.1° on the EISCAT radars). In the EISCAT system, it is normally not possible to find the offset angle. As a way of cataloguing the observed signal strength, we therefore normally quote $\mathrm{RCS}_{\mathrm{min}}$, which we get from Eq. (21) by setting $\phi = 0$.

We note that the energy estimate $W_{\widehat{s}}$, defined in Eq. (9), is a biased estimate. That is, the expectation value $\mathrm{E}\, W_{\widehat{s}}$, over (hypothetical) repeated trials of measurements of the same signal s, is not equal to W_s, the actual signal energy. Instead, in our typical SD measuring situations in EISCAT, $\mathrm{E}W_{\widehat{s}}$ is larger than W_s by as much as a few times the mean noise power σ^2. This is readily seen qualitatively by considering the case when there is no signal present, and thus an unbiased estimate would have zero energy. Because MF^2 is non-negative, $\max \mathrm{MF}^2$ will in any case have expectation value that is larger than zero. But we can actually show that the expectation will be larger than the noise power.

Taking, for definiteness, the model signal to be of the form of (see Eq. (35))

$$\chi(t) = x(t - 2R/c)\mathrm{e}^{i\omega t}\,, \tag{22}$$

where $x(t)$ is transmitted pulse and ω the Doppler shift, the square of the MF becomes

$$\mathrm{MF}^2 = \frac{|\sum \gamma_n x_n \exp i2\pi\nu n|^2}{\sum |x_n|^2} \tag{23}$$

$$= \frac{\sum_{nn'} \gamma_n \overline{\gamma'_n} x_n \overline{x}'_n \exp[i2\pi\nu(n-n')]}{\sum |x_n|^2} \,. \tag{24}$$

Assuming that the noise is uncorrelated, so that

$$\mathrm{E}[\gamma_n \gamma'_n] = \delta_{n,n'} \cdot \sigma^2, \tag{25}$$

we get from Eq. (24)

$$\mathrm{E}[\mathrm{MF}(\theta)^2] = \sigma^2 \text{ , for all } \theta \,. \tag{26}$$

Thus, in most measurements without signal, $\mathrm{MF}(\theta)^2$ varies on both side of σ^2, especially, gets values that are larger than σ^2. Thus the expected value of MF^2 at the maximum position will be larger than σ^2. How much larger, depends on the statistical properties of the noise, the number of parameter space included in the maximization search, and also on the set of model functions used.

The positive bias in the energy estimate means that we tend to overestimate radar cross section when we use $W_{\hat{s}}$ in Eq. (21) without correction.

5 Receiver effects

The MF-method provides an estimate of the energy-to-noise ratio $\mathrm{SNR_N}$ for signal and noise which have been processes through the space debris receiver. But to start estimating the target cross section, we need an estimate of the signal energy *before* the signal has been "corrupted" by the receiver. The noise which enters into the $\mathrm{SNR_N}$ estimate has come through the same receiver path as the signal. Nevertheless, there is in general no guarantee that the (relatively wideband) noise is attenuated by the same amount in the receiver than the signal, which typically consists of a few relatively narrowband frequency channels, transmitted cyclically.

In the standard EISCAT data handling, the receiver effects are taken into account by incorporating the receiver impulse response [5] into the estimation

[5] Normally, only the impulse response of the post-detection filters is incorporated. But in the SD receiver, the receiver bandwidth can be up to 25% of the width of

theory, in the model functions to be fitted. We might ultimately need to do so for the space debris data analysis also. But in this paper, we try to keep the theory simpler by ignoring the receiver response in the model functions. The price is that we need to be prepared to correct the estimated energy. It turns out that for our most common measuring configuration, the estimated energy of the processed signal (relative to noise power) is about 75% of the value in front of the receiver.

For small spherical targets the radar cross section, and therefore the received power, varies proportionally to the six'th power of the target diameter. Thus, a 30% underestimate of received power results only in 5% underestimate of the effective diameter. Considering other serious problems that we have in determining the targets' radar cross section, we have so far simply ignored the receive effect on energy estimate. The other problems include us not knowing the efficiency of the coherent integration (that is, how coherent the "coherent integration" actually is); the problem of not knowing the position of the target within the radar beam; and the problem of (not) knowing accurately the radar's transmitted power.

Ignoring the receiver impulse response is not expected to effect velocity estimate. As of the range estimate, the filter causes a "filter delay" of the order of the sampling interval (0.5–2 μs in our case), and this would in many systems shift the estimated range. But because our model functions are constructed from the actually measured transmission sample signal, and that signal travels though the same receiver path as the target echo, the filter delay should not be an issue.

6 Signal model

We will model the phase of the received signal $s(t)$ by assuming that the phase behaves as if the signal would reflect from a mirror which moves with constant radial acceleration a_0. We will assume that during an integration time T_c, which typically is about 300 ms, the amplitude b of the signal stays constant. Denoting by $x(t)$ the transmitted signal, and by t' the delayed time, with reference to Fig. 3 we take

$$s(t) = bx(t')\,. \tag{27}$$

the IF2 band, and then the IF2 band shape cannot be automatically ignored.

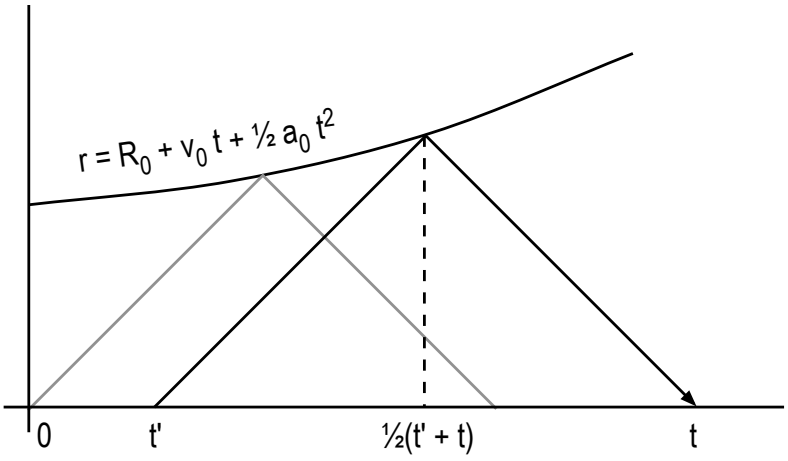

Fig. 3. Pulse reflection from an accelerating target.

For any given target radial motion $r(t)$, the delayed time for reflection from a point target is determined by

$$t - t' = \frac{2r(\frac{t'+t}{2})}{c} \,. \tag{28}$$

With constant radial acceleration, the motion is

$$r = r(R_0, v_0, a_0; t) = R_0 + v_0 t + \frac{1}{2} a_0 t^2 \,. \tag{29}$$

For the motion (29), Eq. (28) is quadratic in t'. Solution of the equation for the pulse propagation time $t - t'$, with appropriate choice of the sign of the square root, is

$$t - t' = \frac{2c}{a_0} \left\{ 1 + \frac{v_0}{c} + \frac{a_0}{c} t - \left[1 + \frac{2v_0}{c} + \left(\frac{v_0}{c} \right)^2 + \frac{2a_0}{c} (t - \frac{R_0}{c}) \right]^{\frac{1}{2}} \right\} \,. \tag{30}$$

Equation (30) can be simplified by expanding the square root to power series. Care must be excised regarding to which terms can be dropped from the expansion. With parameter values that are typical at EISCAT UHF when antenna is pointed near vertically,

$$\begin{aligned} R_0 &\approx 10^6 \text{ m} \,, \\ v_0 &\approx 10^3 \text{ m}s^{-1} \,, \\ a_0 &\approx 10^2 \text{ ms}^{-2} \,, \\ \omega_1 &\approx 6 \cdot 10^9 \text{ Hz} \,, \end{aligned}$$

all terms following the "1" inside the square brackets in Eq. (30) are quite small compared to unity. But what actually determines which terms X we need to keep, is the requirement that the corresponding phase factor $\omega_1 \frac{2c}{a_0} X$, where ω_1 is the radar transmission frequency, stays small during the integration time. Using the first three terms of the power series expansion of $[1+(\ldots)]^{\frac{1}{2}}$, and then dropping all the individual terms for which the corresponding phase factor is less than 0.1 rad when integration time is less than a second, we are left with

$$t - t' \approx \frac{2}{c}\left[R_0 + v_0 t + \frac{1}{2}a_0 t^2 - (v_0 + a_0 t)\frac{R_0}{c}\right] \tag{31}$$

$$= \frac{2}{c}\left[R_0 + v_0(t - \frac{R_0}{c}) + \frac{1}{2}a_0(t - \frac{R_0}{c})^2\right] \tag{32}$$

$$= \frac{2}{c} r(t - \frac{R_0}{c})\,. \tag{33}$$

The term $\frac{-R_0}{c}$ is a natural first order correction to the time instant of pulse reflection; the only non-trivial aspect is that this correction already is sufficient (for our typical measuring configurations). Thus, the model functions $\chi(R, v, a; t)$ to be used in the MF-computation, Eq. (10), are of the form

$$\chi(R, v, a; t) = x(t - \frac{2}{c}\, r(R, v, a;\, t - \frac{R}{c}))\,. \tag{34}$$

Note that has been assumed about the transmission $x(t)$ in this derivation so far. In principle, as long as the transmission can be accurately measured via the transmission sample signal, we do not even need (ever) know what transmission has been used; the MF-machinery incorporates the transmission transparently. This is a good thing for automated piggy-back measurements, where we do not have any control on the transmission EISCAT might be using at any given time.

The reality, of course, is rather different. A basic problem is that the radar's noise-environment is often poorly approximated by our assumption that it consists only of stationary gaussian noise. All kind of distortions happen in practice, one of them being the ionosphere becoming visible as clutter in our data. More or less ad hoc, manual, experiment-specific solutions are used to counter these problems. Also, we cannot at the moment at all handle the case that the antenna pointing may change during a measurement; many EISCAT measurements use cyclical antenna pointing schemes. In practice, both now, and into the foreseeable future, we need to know a priori, and even select, the EISCAT measurements we are making use of in the SD work.

7 Computational aspects

Here we derive the approximation for the signal model that we have been using in our work so far. Assume that transmission can be described as

$$x(t) = \epsilon(t)\mathrm{e}^{i\omega_1 t}\,, \tag{35}$$

where ω_1 is the carrier frequency, and the transmission envelope $\epsilon(t)$ is a slowly changing function, describing, say, binary phase modulation, as is often the case in EISCAT. This description is good for a single-frequency-channel transmission. We drop the correction $-R/c$ to the pulse reflection time in Eq. (34), and use the special form Eq. (35) of transmission to write the model function as

$$\chi(t) \approx \epsilon(t - \frac{2}{c}r(t))\, e^{i\omega_1[t-\frac{2}{c}r(t)]}\,. \tag{36}$$

Inside the slowly varying transmission envelope, we can assume $r(t)$ stays constant, $2R/c$, during the integration time. Then, from Eq. (36) and Eq. (35),

$$\begin{aligned}\chi(t) \approx & \epsilon(t - \frac{2R}{c})\, \mathrm{e}^{i\omega_1(t-\frac{2}{c}R)}\, \mathrm{e}^{i[(-\omega_1\frac{2}{c}v)t+(-\omega_1\frac{a}{c})t^2]} \\ = & x(t - \frac{2R}{c})\, \mathrm{e}^{i(\omega_\mathrm{D}t+\alpha_\mathrm{D}t^2)}\,,\end{aligned} \tag{37}$$

where $\omega_\mathrm{D} = -\omega_1\frac{2v}{c}$ and $\alpha_\mathrm{D} = -\omega_1\frac{a}{c}$ are the Doppler frequency and Doppler drift, respectively. The approximation (37) is often used in the literature (usually without the drift term), and is described by saying that the received signal is delayed-in-time, Doppler-shifted replica of the transmission. With the model (37), the match function definition in Eq. (10) can be expanded for continuous-time signals as

$$\mathrm{MF}(R, v, a) = \frac{|\int_0^{T_\mathrm{c}} z(t)\overline{x}(t - \frac{2R}{c})\mathrm{e}^{-i(\omega_\mathrm{D}t+\alpha_\mathrm{D}t^2)}\, dt|}{\sqrt{W_\mathrm{x}}}\,, \tag{38}$$

where $W_\mathrm{x} = \int |x(t)|^2 dt$ is the energy of the transmission sample signal.

For signal vectors, we need to take into account that transmission samples x_n are only available at times $n\tau$. This already forces us to discretize the range variable. With

$$R_j = j \cdot \frac{c\tau}{2} \tag{39}$$

the match function becomes

$$\mathrm{MF}(R_j, v, a) = \frac{|\sum_{n=0}^{N-1} z_n \overline{x}_{n-j} \mathrm{e}^{-i(\omega_\mathrm{d} n + \alpha_\mathrm{d} n^2)}|}{\|x\|}\,, \tag{40}$$

where the normalized Doppler-shift and Doppler-drift are

$$\omega_\mathrm{d} = -\omega_1 \tau \frac{2v}{c}\,, \tag{41}$$

$$\alpha_\mathrm{d} = -\omega_1 \tau \frac{a\tau}{c}\,. \tag{42}$$

At the points

$$v_k = k \frac{c}{\omega_1 T_\mathrm{c}} \tag{43}$$

Eq. (40) can be written as

$$\mathrm{MF}(R_j, v_k, a) = \frac{|\sum_{n=0}^{N-1} (z_n \overline{x}_{n-j} \mathrm{e}^{-i\alpha_\mathrm{d} n^2}) \mathrm{e}^{-i\frac{kn}{N}}|}{\|x\|}\,, \tag{44}$$

which shows that at these points the MF can be evaluated using FFT. The denominator $\|x\|$ is the square root of transmission sample energy, and is of course independent of R, v and a.

In most of our data analysis, we have taken the radial acceleration to be a deterministic function of range, $a = a(R)$. We have used the acceleration that corresponds to target being on circular orbit and the antenna being pointed vertical,

$$a = g_0 \cdot \frac{R_E}{h} \cdot (\frac{R_E}{R_E + h})^2, \tag{45}$$

where R_E is the Earth radius 6360 km, g_0 is acceleration of gravity at zero altitude, 9.8 m s^{-2}, and h is the target altitude. Experimentation with data has shown that not much sensitivity is lost in practice even if the acceleration is not varied [6].

[6] Which is perhaps a bad thing, because a priori, we would expect the MF to be rather sensitive to the acceleration being correct. For instance, by inspecting the acceleration ambiguity function, $a \to \mathrm{AF}(R_0, v_0, a_0; R, v, a)$, with R and v fixed to the correct values R_0 and v_0, with 0.3 s integration time, an 5 m s^{-2} error in a should cause the coherently integrated amplitude to drop by 70% from the ideal case. That this appears not to happen when we vary the acceleration in the analysis

In our routine analysis therefore, we search the MF-maximum only over the (R_j, v_k)-grid. Even then, the detection computation, using full resolution and without any further approximation, becomes too large. Assume we want to cover 1000 km in range and use 0.3 s coherent integration. Assume that the sampling interval is 0.5 μs. Then input data vector is 600,000 points long, and the FFT requires about 60 Mflops. The $1000/0.075 \approx 13\,000$ range gates require about 800 Gflops. On a G5 workstation, we get about 2 Gflop/s performance on FFTs of this length, so will need about 400 s to handle the 0.3 s of data. Normal EISCAT UHF-radar phase-coded transmissions use code baud lengths typically about 20 μs. For these modulations, we can safely relax the range resolution in the detection phase somewhat, say by a factor of 10 (this also still ensures sufficient Doppler coverage). But this still leaves us more than two orders of magnitude short of real-time speed.

8 The fast match function algorithm

Here we present a fast though approximative way to evaluate MF in Eq. (44), for the purpose of finding the maximum of MF, good for detection purposes. It is sufficient to get a reasonable approximation near the MF maximum position. We make use of two special properties of our measuring situation in EISCAT.

First, we note that the Doppler-velocity range that we need to monitor is much narrower than the range that is actually available with the high sampling rate f_s of about 1 M sample per second. For the 930 MHz radar frequency (0.15 m wavelength), our "bencmark" 2 MHz sampling gives unambiguous velocities in the interval $\pm(f_s/2)\cdot(\lambda/2) = \pm 75$ kms^{-1}. Typically, for near-vertical pointing, we seek to monitor velocity interval ± 5 kms^{-1}. Therefore, we can resample (decimate) the to-be-Fourier-transformed vector in Eq. (44),

$$z_n \overline{x}_{n-j} \mathrm{e}^{-i\alpha n^2} = w_n \,, \tag{46}$$

by a factor M_{dec}, $75/5 = 15$ with 2 MHz sampling. This we do by forming a new sequence w'_n by adding w_n's in blocks of M_{dec}. At the same time, we make use of the fact that within such a block, the acceleration factor $\mathrm{e}^{-i\alpha_{\mathrm{d}} n^2}$ is almost constant. We take it to be a constant, and take it out of the decimation sum, to reduce both the number of multiplications, and the number of complex exponentials that need to be computed.

Second, we make use of the fact that most of w is zeros. The transmission duty cycle in EISCAT experiments is about 10% in the UHF and about 20%

---

of real data, may indicate that there are other factors that are causing the signal model being non-ideal to begin with.

at ESR. Therefore, about 80–90% of w is zeros, in regularly placed blocks. Now we cut out the zero-blocks from w (w'), to form a vector w'' that is typically two orders of magnitude shorter than w. In our benchmark case, w'' has length length $(1/15) \cdot 0.1 \cdot 600,000 = 4000$. Finally, we compute FFT from w'', and use the result in the denominator of Eq. (44),

$$\mathrm{FMF}(R_j, v_k, a) = \frac{|\sum_{n=0}^{N-1} w''_n \mathrm{e}^{-i\frac{kn}{N}}|}{\|x\|}\,. \tag{47}$$

This is the fast match function algorithm. Due to the much shorter FFT input vector, in typical cases the FMF is 100–300 times faster than the standard MF.

That we gain speed by the FMF-algorithm is not in doubt. But what is the price? Decimation, the first step in the algorithm, does not lose us much information. Basically, we are just backtracking from our initial oversampling. We can backtrack at this stage, because the signal w has already been demodulated. Reception is multiplied by complex conjugate of transmission, so the carriers cancel out. Very near the MF maximum, also a possible phase modulation is cancelled out. So the sampling requirement of w is determined by the size of the anticipated maximum Doppler-shit only.

We now inspect the second step. What effect does throwing away the zero-blocks have to the Fourier transform? We consider the original w, ignoring the decimation step. We are interested in the behaviour of the MF near its the maximum. Thus, we will assume that correct range and acceleration have already been found, and only a Doppler-term $e^{i\omega_0 n}$ in w still needs to be cancelled (matched). We ignore noise, so we really are computing what we might, for consistency of the nomenclature, call the "fast ambiguity function", FAF.

We assume that transmission consists of M pulses of length L samples each, sent P samples apart. Then, near the maximum, w consists of M boxcar pulses of, say, unit amplitude and L samples each, Doppler-shifted by the normalized frequency ω_0, with $P - L$ zeros between each pair of pulses. The non-zero part of w consists of m blocks, and in the m'th block, w has values

$$w_n^{(m)} = e^{i\omega_0(n+mP)},\ n = 0, \ldots, L-1. \tag{48}$$

For computing FAF at velocity point $v \leftrightarrow \omega$, instead of just at the FFT points, the blocks $\{w_n^{(m)}\}$ are concatenated, and multiplied by $\mathrm{e}^{-i\omega n}$. The m'th block gets multiplied by

$$u_n^{(m)} = \mathrm{e}^{-i\omega(n+mL)},\ n = 0, \ldots, L-1\,. \tag{49}$$

The contribution I_m of the m'th block to the inner product in the nominator of Eq. (47) is

$$I_m = \sum_{n=0}^{L-1} w_n^{(m)} \cdot u_n^{(m)} \,. \tag{50}$$

The norm $\|x\|$ in the denominator of Eq. (47) is sum of ML terms all equal to unity, so we get from Eq. (47) and (50)–(48)

$$\begin{aligned}
\mathrm{FAF}(\omega) &= \frac{1}{ML} \left| \sum_{m=0}^{M-1} I_m \right| && (51)\\
&= \frac{1}{ML} \left| \sum_m \sum_n \mathrm{e}^{i\omega_0(n+mP)} \mathrm{e}^{-i\omega(n+mL)} \right| && (52)\\
&= \frac{1}{L} \left| \sum_{n=0}^{L-1} \mathrm{e}^{i(\omega_0-\omega)n} \right| \cdot \frac{1}{M} \left| \sum_{m=0}^{M-1} \mathrm{e}^{i(\omega_0 P-\omega L)m} \right| && (53)\\
&= \mathrm{diric}(\omega_0-\omega, L) \cdot \mathrm{diric}(\omega_0 P - \omega L, M) \,, && (54)
\end{aligned}$$

where the "Dirichlet kernel" is

$$\mathrm{diric}(x, M) = \left| \frac{\sin xM/2}{M \sin x/2} \right| \,. \tag{55}$$

The first factor in Eq. (54) encodes the Doppler-information available from a single pulse. The function has absolute maximum at the target Doppler-frequency ω_0, and first zeros at $\omega_\pm = \omega_0 \pm 2\pi/L$. The second factor in Eq. (54) results from pulse repetition. It has maxima, equal to unity, at the points

$$\omega_n = \frac{P}{L}\omega_0 + n\frac{2\pi}{L} \,. \tag{56}$$

In general, none of the maxima ω_n coincides with ω_0. Therefore, the maximum of $\mathrm{FAF}(\omega)$ is not situated in the "correct" place ω_0, even now when there is no noise. This mean that (with noise), the estimated velocity would be said to be "biased". This is not serious. The bias is rather small, less than 0.2 kms^{-1} in our typical measurement modes. For some values of the target velocity, the bias vanishes, and anyway, is deterministic and could be corrected for (modulo a rather serious velocity ambiguity, ultimately deriving from the infamous range-Doppler ambiguity).

What is more important for detection, is the loss of maximum signal amplitude. The maximum value of the FAF occurs (very near) that ω_n which is nearest to ω_0. Such an ω_n, according to Eq. (56), is never further away from

ω_0 than half the spacing $2\pi/L$ between the ω_n's. Therefore, the FAF maximum value, in the worst case, is roughly equal to $\mathrm{diric}(\pi/L, L) \approx 2/\pi = 64\%$, of the ideal value.

When we use FFT, and only evaluate FAF at a discrete set of points v_k, the worst-case maximum value can get worse by another factor of 0.6 due to the "picket-fence" effect. On the other hand, we normally can observe a target for several seconds, and during that time, its velocity, hence ω_0, typically changes so much that during some integration period, the FMF maximum gets nearer to the ideal value. This partially explains why we in practice get almost the same detection sensitivity when we use FMF as when we use the standard MF. The main difference seems to be that detection with the FMF goes a few hundred times faster.

9 Acknowledgements

The EISCAT facility is supported by Finland (SA), France (CNRS), the Federal Republic of Germany (MPG), Japan (NIPR), Norway (NFR), Sweden (NFR), and the United Kingdom (PPARC).

References

M. Baron, The EISCAT facility, *J. atmos. terr. Phys.* **46** (1984) 469.

M. Baron, EISCAT progress 1983–1985, *J. atmos. terr. Phys.* **48** (1986) 767.

ESA Directorate of Technical and Operational Support ESOC Ground Segment Engineering Department Mission Analysis Section, *Study specification, measurements of small-size debris with backscatter of radio waves* (Darmstadt, Germany, 1999).

ESA Directorate of Technical and Operational Support ESOC Ground Segment Engineering Department Mission Analysis Section, *Study specification, real-time space debris detection with EISCAT radar facilities* (Darmstadt, Germany, 2002).

M. Lehtinen, Statistical theory of incoherent scatter radar measurements, *EISCAT Techn. Note* **86/45** (Eur. Incoherent Scatter Sci. Assoc., Kiruna, Sweden, 1986).

M. Lehtinen, J. Markkanen, A. Väänänen, A. Huuskonen, B. Damtie, T. Nygren and J. Rahkola, The EISCAT Svalbard radar: A case study in modern incoherent scatter radar system design, *Radio sci.* **32** (1997) 2283.

B. R. Mahafza, *Radar system analysis and design using MATLAB* (Chapman-Hall/CRC, 2000).

J. Markkanen, M. Lehtinen, A. Huuskonen and A. Väänänen, Measurements

of Small-Size Debris with Backscatter of Radio Waves, (Final Report, ESOC Contract No. 13945/99/D/CD, March 2002).

M. I. Skolnik, *Introduction to radar systems* (second edition, McGraw-Hill, Singapore, 1981).

G. Wannberg, I. Wolf, L.-G. Vanhainen, K. Koskenniemi, J. Röttger, M. Postila, J. Markkanen, R. Jacobsen, A. Stenberg, R. Larssen, S. Eliassen, S. Heck and A. Huuskonen, The EISCAT Svalbard radar: A case study in modern incoherent scatter radar system design, *Radio sci.* **32** (1997) 2283.